COMMUNICATION

Advancing MIM Electronics: Amorphous Metal Electrodes

*E. William Cowell III, Nasir Alimardani, Christopher C. Knutson, John F. Conley Jr., Douglas A. Keszler, Brady J. Gibbons, and John F. Wager**

Effectively controlling quantum mechanical tunneling through an ultrathin dielectric represents a fundamental materials challenge in the quest for high-performance metal-insulator-metal (MIM) diodes. Such diodes are the basis for alternative approaches to conventional thin-film transistor technologies for large-area information displays,[1,2] various types of hot electron transistors,[2–6] ultrahigh speed discrete or antenna-coupled detectors,[7–14] and optical rectennas.[15] MIM diodes have been fabricated by anodization,[1] thermal oxidation,[8–11,14] plasma oxidation,[10,12,13] or plasma nitridation[16] of crystalline metal films. Diodes fabricated using these approaches have invariably exhibited poor yield and performance. These problems are to a large extent a consequence of the roughness of the surface of the crystalline metal film, which is often larger than the thickness of the MIM insulator. As a result, the electric field across a MIM device will be highly nonuniform, making the control of quantum mechanical tunneling problematic. In this contribution, we describe the use of an amorphous metal contact as a critical component for circumventing the surface roughness and field uniformity roadblocks that have precluded the realization and utility of MIM electronics for applications requiring high device current rectification ratios (e.g. display applications).

The MIM diode is the fundamental building block of metal-insulator electronics. The device is characterized by a high degree of nonlinearity in its current-voltage characteristics as a result of a large difference in conductivity between on and off states. The operational theory of this diode, based on Fowler-Nordheim tunneling, has been described in detail by Simmons.[17,18] The probability of quantum mechanical tunneling depends exponentially on the thickness of the insulator between a pair of metal electrodes. Hence, the performance of the diode is critically dependent on the thickness uniformity of the tunnel-dielectric layer across the entire device. Interfacial roughness and dielectric imperfections give rise to alternate conduction mechanisms, e.g. Frenkel Poole emission, that can dominate at low voltages and reduce the device rectification ratio. The inability to create and effectively control a uniform electric field across the whole device area has been the primary limitation in producing reliable MIM devices. Here, we demonstrate that the necessary field control can readily be achieved by integrating the atomically smooth-surface of an amorphous metal electrode with high-quality insulators. This combination provides a rich materials and processing palette for development of MIM electronics, enabling new strategies for device design and fabrication.

Amorphous metals have been primarily investigated as bulk materials, addressing diverse applications that range from micromachines and hinges for digital light processors to golf clubs and transformer cores.[19–21] They have also been deposited in thin-film form, primarily for study and development of micro-electromechanical systems.[22–27] Relative to crystalline metals, they are more electrically resistive by approximately two orders of magnitude.[28,29] While this resistivity limits their use as interconnects, it is not an impediment to their use as electrodes. To date, however, there have been no reports involving the use of amorphous metal films as electrodes in electronic devices.

Our investigation of amorphous metal films as electrode materials was stimulated by the smooth surfaces reported for the amorphous metal ZrCuAlNi in thin-film form.[25,26] We hypothesized that the availability of such a smooth surface would provide the basis for a flat metal-insulator interface, producing an MIM device with a uniform and homogeneous electric field over large areas. Initial characterization of a ZrCuAlNi film deposited via DC sputtering revealed an rms roughness of ~0.2 nm with maximum excursions to 1.7 nm in an area of 5 μm × 5 μm (**Figure 1a**). For comparison, the rms roughness of a thermally-evaporated crystalline Al film is 5 nm with excursions as high as 70 nm (Figure 1b); this degree of surface roughness is not surprising given the tendency for elemental metals to crystallize, even when deposited at room temperature.[30] Clearly, the ZrCuAlNi amorphous metal film exhibits a much smoother surface than that of a typical crystalline metal. The initial MIM diodes fabricated for electrical characterization are schematically represented in Figure 1c. The devices are built from a blanket coat of 200 nm of a ZrCuAlNi amorphous metal film electrode (M1) on SiO_2, an approximately 10-nm thin film of Al_2O_3 produced by atomic-layer deposition (ALD), and upper electrodes (M2) as arrays of 1-mm diameter dots of ZrCuAlNi or Al metal. As seen in TEM images (Figure 1d and e), the selected materials and processes afford uniform films and well-defined metal/insulator interfaces. Note from Figure 1d and e that a native oxide ~1.5 nm thick is present at the M1/insulator interfaces for both MIM diodes. X-ray

E. W. Cowell III, N. Alimardani, Prof. J. F. Conley Jr., Prof. J. F. Wager
School of Electrical Engineering and Computer Science
Oregon State University
1148 Kelley Engineering Center
Corvallis, OR 97331–5501, USA
E-mail: jfw@eecs.oregonstate.edu
C. C. Knutson, Prof. D. A. Keszler
Department of Chemistry
Oregon State University
153 Gilbert Hall, Corvallis, OR 97331–4003, USA
Prof. B. J. Gibbons
School of Mechanical
Industrial, and Manufacturing Engineering
Oregon State University
204 Rogers Hall, Corvallis, OR 97331–6001, USA

DOI: 10.1002/adma.201002678

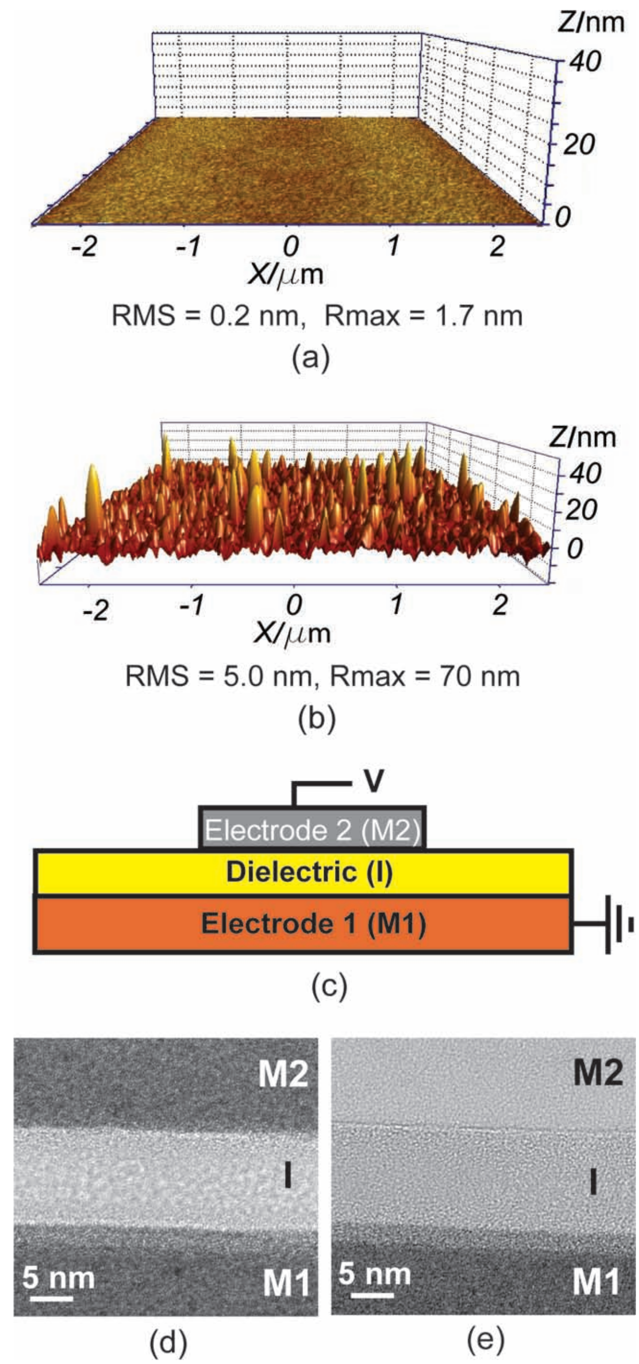

Figure 1. a) An AFM image of the surface of a 100-nm ZrCuAlNi amorphous metal film. b) AFM sectional analysis of the surface of a 150-nm Al blanket. c) Schematic representation of an MIM diode. d) TEM image of an MIM diode; M1 = ZrCuAlNi, I = Al_2O_3, M2 = Al. e) TEM image of an MIM diode; M1 = ZrCuAlNi, I = Al_2O_3, M2 = ZrCuAlNi.

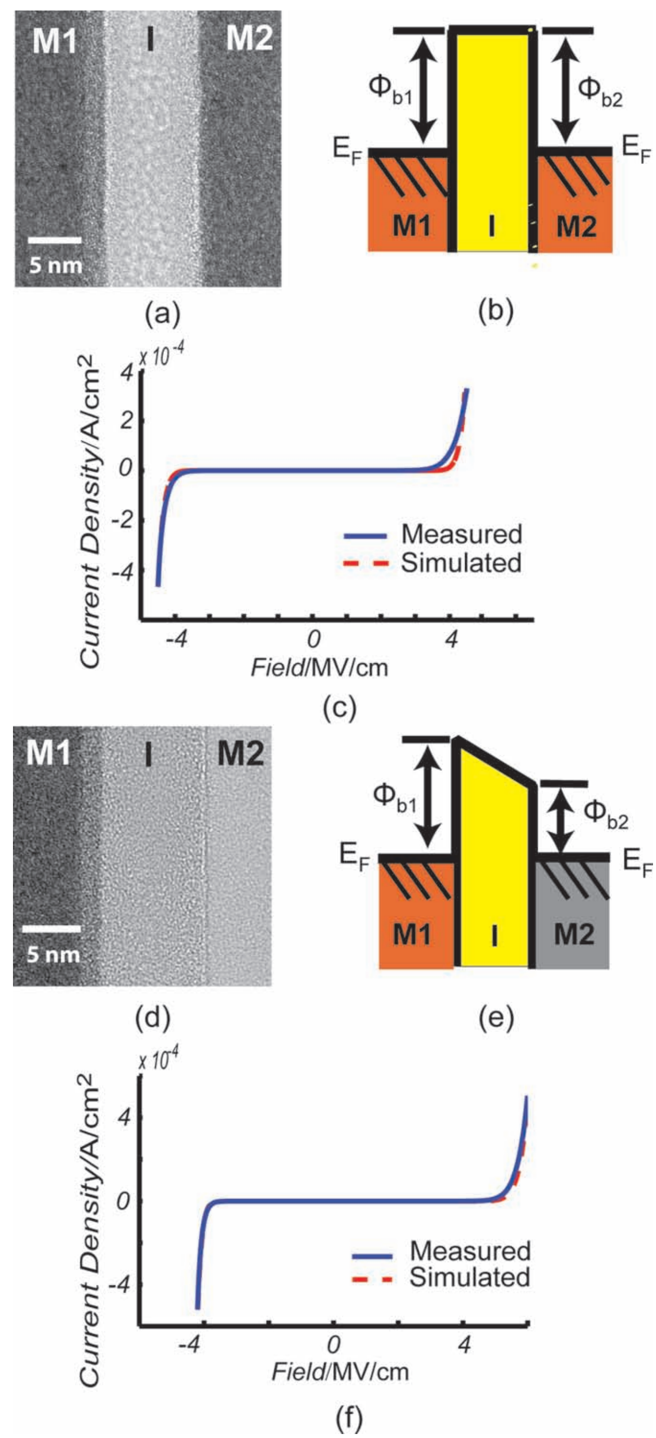

Figure 2. a) TEM image of a symmetric MIM diode fabricated with M1 = ZrCuAlNi amorphous metal film, I = 10 nm Al_2O_3, M2 = ZrCuAlNi amorphous metal film. b) Equilibrium energy-band diagram for a symmetric MIM diode. c) Measured and simulated current density-field (J–ξ) curves for the MIM diode shown in (a). d) TEM image of an asymmetric MIM diode fabricated with M1 = ZrCuAlNi amorphous metal film, I = 10 nm Al_2O_3, M2 = Al. e) Equilibrium energy band diagram for an asymmetric MIM diode. f) Measured and simulated J–ξ curves for the MIM diode shown in (d). A positive electric field corresponds to application of a positive voltage to electrode M2.

photoelectron spectroscopy assessment of this native oxide indicates it to be predominantly ZrO_2.[31]

The MIM diode, constructed using ZrCuAlNi amorphous metal films for both M1 and M2 electrodes, is a symmetric device; the associated equilibrium energy-band diagram is shown in **Figure 2b**. This diode has equivalent barriers

($\varphi_{b1} = \varphi_{b2}$) at the metal/insulator interfaces, giving rise to a symmetric current density-applied electric field (J–ξ) curve (Figure 2c). Symmetric MIM diodes with ZrCuAlNi amorphous metal electrodes have been fabricated with yields >70%. (In contrast, we were unable to fabricate even a single working MIM diode when using 10 nm Al_2O_3 and symmetric evaporated Al electrodes, even though we employed the same high-quality, conformal ALD Al_2O_3 dielectric.) In the amorphous-metal diodes, negligible current flow is observed until the magnitude of the electric field exceeds 3.5 MV/cm. These devices are quite stable as repeated voltage sweeps reveal no hysteresis. This performance is consistent with the high quality of the individual films and the resulting uniform electric fields. These characteristics are particularly noteworthy, considering the relatively large areas of the individual devices (~1 mm^2).

In contrast, the MIM diode with ZrCuAlNi as the lower electrode (M1) and Al as the upper electrode (M2) possesses asymmetric barriers ($\varphi_{b1} > \varphi_{b2}$; Figure 2e), leading to the asymmetric J–ξ curve shown in Figure 2f. As seen in Figure 2f, tunneling currents on the order of microamps occur at fields above 4 MV/cm for negative polarity and above 5 MV/cm for positive polarity, confirming the expected asymmetric behavior. The barrier height asymmetry for this device is approximately 0.8 eV, since the work functions of the ZrCuAlNi and Al metal films are measured via Kelvin probe to be 4.8 and 4.0 eV, respectively. These asymmetric MIM diodes possess desirable yield and performance properties similar to those of the symmetric MIM devices discussed previously, even though the upper Al electrode is crystalline with a normally rough surface (Figure 1b). The roughness of this surface is not relevant, as the insulator/Al interface is smooth due to the planarity of the ALD Al_2O_3. Thus, it appears that the key to obtaining a high-performance MIM diode is to insure that the initial metal surface is ultrasmooth. The TEM image (Figure 2d) reveals sharp and uniform interfaces.

Measured J–ξ curves for symmetric and asymmetric MIM tunnel diodes, as shown in Figure 2c and 2f, can be accurately simulated by using the theory of Simmons,[17,18] confirming that Fowler-Nordheim tunneling indeed dominates at both positive and negative fields. The agreement between measured and simulated J–ξ curves for the asymmetrical MIM tunnel diode (Figure 2f) is particularly good. The simulated symmetrical MIM diode J–ξ curve (Figure 2c) is less satisfying, since a noticeable deviation occurs for the positive polarity, corresponding to additional or greater than predicted electron tunnel injection from the top Al_2O_3/ZrCuAlNi interface. We attribute this discrepancy to the use of DC magnetron sputtering for deposition of the upper ZrCuAlNi electrode. In this process, depositing species have energies on the order of 2–7 eV,[30] which appears to be sufficient to slightly thin and roughen the tunnel insulator (see Figure 2a). In contrast, thermal evaporation, a low-energy process that imparts only thermal energy to the Al_2O_3 tunnel-barrier surface, is employed in the construction of the upper Al electrode in the asymmetric MIM tunnel diode. Here, a much smaller positive polarity difference between measured and simulated J–ξ curves (Figure 2f) is witnessed. The associated TEM image shows the insulator/M2 interface to be pristine (Figure 2d).

Current–voltage (I–V) curves for a series of asymmetric ZrCuAlNi–Al_2O_3–Al MIM diodes with variable tunnel-barrier thicknesses are presented in **Figure 3**. The insulator thickness

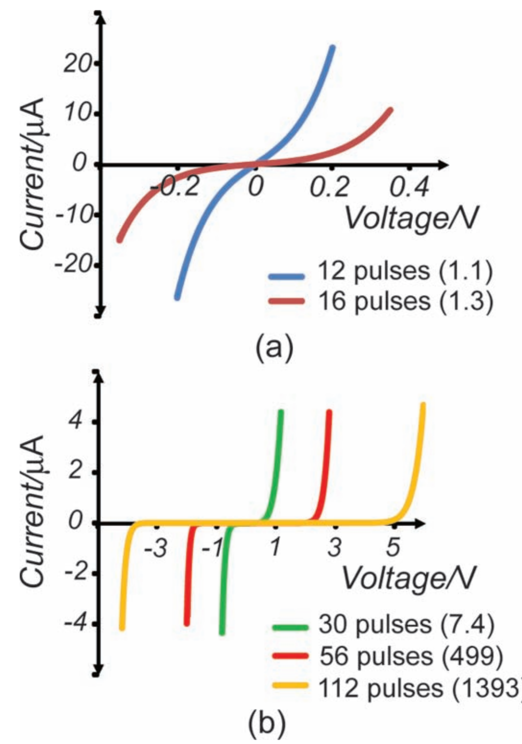

Figure 3. Current-voltage (I–V) curves of asymmetric MIM diodes fabricated with M1 = ZrCuAlNi amorphous metal film, I = Al_2O_3, and M2 = Al. a) I–V characteristics for MIM diodes with ultrathin tunnel barriers (< 2 nm). b) I–V curves for 30, 56, 112 ALD pulses of Al_2O_3. Asymmetry parameters for devices are given in parentheses. A positive voltage corresponds to application of a positive voltage to electrode M2.

is specified in terms of ALD pulse cycles, i.e., alternating purge-separated pulses of trimethlyaluminum and deionized water. As a point of reference, 112 pulse cycles has been measured to correspond to an Al_2O_3 thickness of approximately 10 nm. At a small number of pulse cycles, the thickness of the ALD-deposited Al_2O_3 is difficult to measure. The pulse cycles/thickness relationship becomes less linear as the number of pulse cycles is reduced below 30. In addition, the thickness of the native oxide present on the amorphous metal electrode for the ultrathin deposited layers is an appreciable fraction of the total MIM insulator thickness.

MIM diode applications involving rectification or detection require I–V curves to be asymmetric, if they are to be operated without an offset bias.[11,15] As shown in Figure 3a, diodes with ultrathin Al_2O_3 insulators exhibit nonlinear behavior but very little I–V curve asymmetry. (For comparison, I–V asymmetry is quantitatively defined as the ratio of the positive-to-negative polarity current at an electric-field magnitude of 4 MV/cm. The asymmetry evaluated in this manner is specified in parentheses in Figure 3.) These I–V curves are nearly symmetric, because their insulators are so thin that current from direct tunneling across the insulator dominates at very low applied voltages. (Direct tunneling occurs through a trapezoidal barrier, in contrast to Fowler-Nordheim tunneling through a triangular barrier.) I–V asymmetry is expected to be pronounced only if the insulator is thick enough to stand off significant direct tunneling current up to the onset of

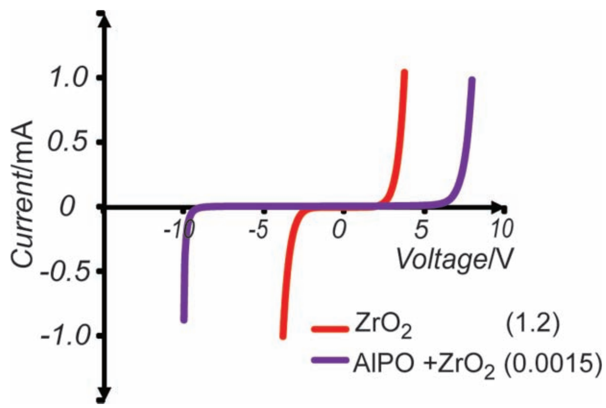

Figure 4. *I–V* curves for MIM diodes with M1 = ZrCuAlNi, M2 = Al, and I = ZrO_2 or AlPO + ZrO_2. The ZrO_2 diode was annealed in air to form the tunnel dielectric. The AlPO + ZrO_2 diode had 10 nm of AlPO deposited onto the surface of the ZrCuAlNi lower electrode and was subsequently annealed in air. Asymmetry parameters for devices are given in parentheses. A positive voltage corresponds to application of a positive voltage to electrode M2.

Fowler-Nordheim tunneling. Figure 3b shows that this changeover occurs between 30 and 56 pulse cycles, where the asymmetry abruptly jumps from 7.4 to 499. Direct tunneling occurs at low voltages for all diodes, regardless of the insulator thickness, and it determines the magnitude of the zero bias resistance. For MIM tunnel diodes fabricated using 112 and 12 ALD pulse cycles, the zero bias resistance is > 10^{11} Ω and 20 kΩ, respectively.

To extend the functionality of amorphous metal films and to simplify MIM diode fabrication, two approaches were explored, leveraging the direct oxidation of the amorphous metal electrode and the ease of solution processing. First, a blanket amorphous metal electrode was annealed in air to thicken the native Zr(IV) oxide (at 300 °C, a temperature that does not promote crystallization of the amorphous metal). After the anneal, Al electrodes were thermally deposited to complete the structure. A representative *I–V* curve for these devices is presented in **Figure 4**. The *I–V* asymmetry of the resulting structure is measured to be 1.2, which is less than that expected from consideration of the differences in electrode work functions. The origin of this discrepancy is under investigation. A second oxidation-based asymmetric MIM diode was fabricated via the incorporation of a solution-deposited aluminum phosphate (AlPO) film[32] as a portion of the tunnel barrier. An MIM structure was realized by spin coating the AlPO film onto the ZrCuAlNi electrode, annealing in air at 300 °C, and then depositing an Al upper electrode. The device exhibits the onset of significant tunneling currents (Figure 4) at voltages higher than those of the devices employing Al_2O_3 films produced via ALD. The asymmetry is 0.0015, indicating that the polarity dependence of the current has switched from that seen for the asymmetric diodes fabricated with the Al_2O_3 tunnel barriers. We have recently reported significant interdiffusion between the interfaces of ZrCuAlNi and AlPO bilayers in nanolaminated structures.[31] The presence of the AlPO layer and its interaction with the native ZrO_2, formed during annealing, creates an opportunity for controlling the I–V polarity dependence of the MIM diode.

In summary, high-performance, high rectification ratio MIM diodes employing amorphous metal electrodes have been demonstrated. ZrCuAlNi amorphous metal film lower electrodes have been coupled with high-quality insulators and ZrCuAlNi and Al upper electrodes to produce uniform electric fields for the successful operation of both symmetric and asymmetric diodes. All diodes were fabricated by using relatively low temperatures (≤300 °C), rapid DC sputtering of the amorphous metal, and ALD or solution processing for deposition of high-quality insulators. Together, these methods provide opportunities for device fabrication on a variety of substrates, extending to large areas. In addition, the exceptionally broad compositional space of amorphous metal films provides unique opportunities to modify work functions and tune barrier heights for control of electron tunneling and device operation. Hence, this approach to MIM electronics presents an intriguing new means both for designing very high-performance electronic devices and integrating them across multiple technology platforms.

Experimental Section

Thin Films: ZrCuAlNi amorphous metal thin films were deposited onto Si/SiO_2 (100 nm SiO_2) substrates using DC magnetron sputtering with no intentional substrate heating at a power of 60 W, a pressure of 3 mTorr, and an Ar flowrate of 20 sccm. A 3-inch diameter, 0.25-inch thick vacuum arc-melted metal target (with an atomic composition $Zr_{40}Cu_{35}Al_{15}Ni_{10}$) fabricated by Kamis Inc. was used for all ZrCuAlNi depositions.

Atomic layer deposition (ALD) of Al_2O_3 was carried out in a Picosun SUNALE R-150B ALD reactor using trimethlyaluminum (TMA) and de-ionized water at a temperature of 300 °C. The pulse durations for both TMA and water were 0.1 s with a 2-s nitrogen purge between pulses. MIM diode structures were completed by shadow masking ~1 mm diameter top contacts deposited by either thermal evaporation of Al or DC magnetron sputter deposition of ZrCuAlNi films using the deposition parameters described above.

The solution-based dielectric depositions were carried out using an aluminum oxide phosphate solution containing a 0.10 M metal concentration at an aluminum-to-phosphorus ratio of 30:18.[32] The solution was deposited via spin-coating for 30 s at a speed of 3000 rpm, followed by rapid heating at 300 °C for 1 min on a hotplate in air. Films were annealed in air at 300 °C.

Atomic force microscope (AFM) measurements were made using a Digital Instruments 3 instrument with silicon-nitride tips; images were acquired over 5 μm × 5 μm areas. Transmission electron microscopy (TEM) images were obtained with a JEOL 2500 TEM from samples prepared with a Dual Beam FEI 235 focused ion beam. Work function measurements were performed in air by using a KP Technology SKP5050 scanning Kelvin probe with a 2-mm tip calibrated against a gold standard. The work function analysis was carried out over an area of approximately 1 mm × 1 mm.

Electrical measurements were performed by using a Hewlett-Packard 4156C semiconductor parameter analyzer. The blanket lower ZrCuAlNi electrode was held at ground potential with bias applied to the upper electrode. A dual-sweep measurement was employed to allow for an assessment of current-voltage curve hysteresis. The magnitude of the applied voltage bias was scaled according to the tunnel-barrier thickness to target maximum current levels in the μA range.

Current Density-Electric Field Simulation: Simulation of current density-electric field (J–ξ) curves was performed with Matlab, using the Fowler-Nordheim tunneling equations developed by Simmons.[17,18] Optimized fits to measured J–ξ curves, as shown in Figure 2, were obtained by using an effective mass between 0.45 to 1.0 of the free electron mass, $\varphi_{bZnCuAlNi} = 2.2 \pm 0.3$ V, $\varphi_{bAl} = 1.3 \pm 0.1$ V, and adjusting the insulator thickness.

COMMUNICATION

Acknowledgements

This material is based upon work supported by the National Science Foundation under grant numbers CHE-0847970 (EWC, DAK, JFW) and DMR-0805372 (JFC) and by the Army Research Laboratory under contract W911NF-07–2-0083 (NA, CCK). The authors thank Peter Eschbach, William Stickle, Ronald Kelley, and Randy Burgess of the ADL at Hewlett Packard, Corvallis, Oregon for the TEM analysis; and Iain Balke of KP Technologies, LTD. for the Kelvin Probe analysis.

Received: July 26, 2010
Published online: October 25, 2010

[1] W. den Boer, in *Active Matrix Liquid Crystal Displays*, Elsevier, Amsterdam, **2005**.
[2] K. K. Ng, in *Complete Guide to Semiconductor Devices*, 2nd Edition, Wiley-Interscience, New York, **2002**.
[3] J. L. Moll, *IEEE Trans. Electron Devices* **1963**, *10*, 299.
[4] S. M. Sze, in *Physics of Semiconductor Devices*, 1st Ed, Wiley-Interscience, New York, **1969**.
[5] *High-Speed Semiconductor Devices* (Ed: S. M. Sze), Wiley-Interscience, New York, **1990**.
[6] S. M. Sze, K. K. Ng, in *Physics of Semiconductor Devices*, 3rd Edition, Wiley-Interscience, Hoboken, New Jersey, **2007**.
[7] S. P. Kwok, G. I. Haddad, G. Lobov, *J. Appl. Phys.* **1971**, *42*, 554.
[8] G. M. Elchinger, A. Sanchez, C. F. Davis, A. Javan, *J. Appl. Phys.* **1976**, *47*, 591.
[9] M. Heiblum, S. Wang, J. R. Whinnery, T. K. Gustafson, *IEEE J. Quantum Electron.* **1978**, *14*, 159.
[10] M. Brunner, H. Ekrut, A. Hahn, *J. Appl. Phys.* **1982**, *53*, 1596.
[11] E. N. Grossman, T. Harvey, C. D. Reintsema, *J. Appl. Phys.* **2002**, *91*, 10134.
[12] P. C. D. Hobbs, R. B. Laibowitz, F. R. Libsch, *Appl. Optics* **2005**, *44*, 6813.
[13] S. Krishnan, E. Stefanakos, S. Bhansali, *Thin Solid Films* **2008**, *516*, 2244.
[14] J. A. Bean, B. Tiwari, G. H. Bernstein, P. Fay, W. Porod *J. Vac. Sci. Technol. B* **2009**, *27*, 11.
[15] B. Berland, National Renewable Energy Laboratory Final Report, **2003**, see: http://www.nrel.gov/docs/fy03osti/33263.pdf.
[16] G. Lewicki, C. A. Mead, *Phy. Rev. Lett.* **1966**, *16*, 939.
[17] J. G. Simmons, *J. Appl. Phys.* **1963**, *34*, 1793.
[18] J. G. Simmons, *J. Appl. Phys.* **1963**, *34*, 2581.
[19] H. Warlimont, *Mater. Sci. Eng. A* **2001**, *304*, 61.
[20] J. Tregilgas, *Adv. Mater. Proc.* **2005**, *163*, 46.
[21] A. Greer, E. Ma, *MRS Bull.* **2007**, *32*, 611.
[22] S. Hata, K. Sato, A. Shimokohbe, *Proc, SPIE* **1999**, *3892*, 97.
[23] Y. Liu, S. Hata, K. Wada, A. Shimokohbe, *Jpn. J. App. Phys.* **2001**, *40*, 5382.
[24] J. P. Chu, C. T. Liu, T. Mahalingam, S. F. Wang, M. J. O'Keefe, B. Johnson, C. H. Kuo, *Phys. Rev. B* **2004**, *69*, 113410.
[25] P. Sharma, W. Zhang, K. Amiya, H. Kimura, A. Inoue, *J. Nanosci. Nanotechnol.* **2005**, *5*, 416.
[26] P. Sharma, N. Kaushik, H. Kimura, Y. Saotome, A. Inoue, *Nanotechnology* **2007**, *18*, 035302.
[27] F. X. Liu, P. K. Liaw, W. H. Jiang, C. L. Chiang, Y. F. Gao, Y. F. Guan, J. P. Chu, P. D. Rack, *Mater. Sci. Eng. A* **2007**, *468*, 246.
[28] N. F. Mott, in *Conduction in Non-Crystalline Materials*, Oxford University Press, Oxford, **1993**.
[29] J. Dugdale, in *The Electrical Properties of Disordered Metals*, Cambridge University Press, Cambridge **2005**.
[30] M. Ohring, in *Materials Science of Thin Films*, 2nd Ed., Academic Press, San Diego, **2001**.
[31] E. W. Cowell III, C. C. Knutson, J. F. Wager, D. A. Keszler, *Appl. Mater. Interfaces* **2010**, *2*, 1811
[32] S. T. Meyers, J. T. Anderson, D. Hong, C. M. Hung, J. F. Wager, D. A. Keszler, *Chem. Mater.* **2007**, *19*, 4023.